Journal of Applied Fluid Mechanics, Vol. 17, No. 1, pp. 219-232, 2024.
Available online at www.jafmonline.net, ISSN 1735-3572, EISSN 1735-3645.
https://doi.org/10.47176/jafm.17.1.1994

Suppressing the Vortex Rope Oscillation and Pressure Fluctuations by the Air Admission in Propeller Hydro-Turbine Draft Tube

H. Wu[1], F. Jin[1], Y. Luo[1†], Y. Ge[2], Q. Wei[2], C. Zeng[3], X. Liu[3], W. Zhang[2], D. Miao[2] and H. Bai[2]

[1] *Department of Energy and Power Engineering, Tsinghua University, Beijing, 100084, China*
[2] *Huaneng Liaoning Clean Energy CO. Ltd, Shenyang, 110167, China*
[3] *Huaneng Clean Energy Research Institute, Beijing, 102209, China*

†*Corresponding Author Email: luoyy@mail.tsinghua.edu.cn*

ABSTRACT

For the purpose of automatic generation control (AGC), a portion of the propeller hydro-turbine units in China is adjusted to operate within a restricted range of 75%-85% load using computer-controlled AGC strategies. In engineering applications, it has been observed that when a propeller hydro-turbine unit operates under off-design conditions, a large-scale vortex rope would occur in the draft tube, leading to significant pressure fluctuations. Injecting air into the draft tube to reduce the amplitude of pressure fluctuations is a common practice, but its effectiveness has not been proven on propeller hydro-turbine units. In this study, a CFD model of a propeller hydro-turbine was established, and 15 cases with different guide vane openings (GVO, between 31° and 45°) under unsteady conditions were calculated and studied. Two air admission measures were introduced to suppress the vortex rope oscillation in the draft tube and to mitigate pressure fluctuations. The reason for the additional energy loss due to air admission was then explained by the entropy production theory, and its value was quantified. This study points out that when injecting air, it is necessary to first consider whether the air will obstruct the flow in the draft tube. Finally, based on simulation and experimental data under various load conditions, pressure fluctuation analysis (based on fast Fourier transform, FFT) was conducted to assess the effectiveness of air admission measures. This study can provide an additional option for balancing unit efficiency and stability when scheduling units using an AGC strategy.

Article History

Received May 9, 2023
Revised September 7, 2023
Accepted September 12, 2023
Available online November 1, 2023

Keywords:

Propeller hydro-turbine
Computational fluid dynamics
Vortex rope
Pressure fluctuation
Air admission
Entropy production theory

1. INTRODUCTION

The power system requires reliable generation equipment to achieve stable operation. In order to produce high-quality electricity while reducing environmental pollution, achieving energy conservation and carbon neutrality (Yu et al., 2021a), hydropower has become a prominent option that needs to be vigorously developed, due to its high energy density, power generation efficiency, and stability (Pasche et al., 2017). Furthermore, hydropower units can rapidly respond to grid demands, thereby assisting in AGC (Goyal & Gandhi, 2018; Mao et al., 2021). To ensure the integration of intermittent non-fossil energy sources such as wind and solar power into the grid successfully, and enhance the stability of the power system, increasing the scale of hydropower generation is crucial (Ardizzon et al., 2014). An adequate installed capacity of hydropower can ensure that electricity production and consumption are balanced within the power system (Li et al., 2018).

Propeller hydro-turbine units are usually adopted to generate electricity in low-head or low-head variation water flow conditions (Krzemianowski & Kaniecki, 2023; Sunsheng et al., 2023). The propeller hydro-turbine is distinguished by its maximum discharge capacity, which exceeds that of the Francis turbine at the same head condition. Nonetheless, the runner blade angle of the hydro-turbine cannot be adjusted, resulting in a highly variable efficiency curve in the experiment's hill chart, rendering it unsuitable for installation in hydropower stations with significant head variations. Head conditions at some hydropower stations have been altered by early construction, and thus these units are often operated under off-design conditions. Furthermore, in some small hydropower stations in China, some hydro-turbines intentionally generate electricity using smaller water

NOMENCLATURE

AGC	Automatic Generation Control	$\vec{V}$	time-averaged relative velocity
CFD	Computational Fluid Dynamics	α	volume fraction of vapor
D	runner diameter	β	model constants
FFT	Fast Fourier Transform	β^*	model constants
f_n	rotating frequency of runner	μ	dynamic viscosity
GVO	Guide Vane Opening	μ_t	turbulent eddy viscosity
k	turbulent kinetic energy	ρ_w	density of water
P	production term	σ_k	model constants
Q	rated discharge	σ_ω	model constants
RANS	Reynolds-Averaged Navier-Stokes	τ	torque of runner
$S_{\bar{D}}^{\prime\prime\prime}$	direct dissipation	ω	dissipation rate
$S_{D'}^{\prime\prime\prime}$	indirect dissipation	$\vec{\omega}$	relative vorticity
$S_{D'}$	entropy induced by the fluctuating velocity		

Flows (75%-85% rated power) for AGC purposes, thereby causing the units to operate in partial load conditions (Pasche et al., 2017). These off-design conditions can cause the units to extra vibrate, posing a risk to the hydropower station's stability and safety (Luo et al., 2013; Liu et al., 2018).

Prior studies have demonstrated that the flow within propeller hydro-turbines during part-load operation becomes notably intricate. Specifically, a spiral vortex rope emerges inside the draft tube cone, which can induce significant pressure fluctuations within the hydro-turbine units (Zhang et al., 2009; Pasche et al., 2017). Consequently, this can impede the efficiency of the hydro-turbine and jeopardize the stability of the hydropower unit. The vortex rope is a cavitation phenomenon within a draft tube, and it is a low-pressure area that is difficult to mitigate. (Gohil & Saini, 2016; Luo et al., 2016). When the vortex rope rotates inside the draft tube with the rotation of the runner, it interacts with the draft tube wall, causing vibration and hindering the normal flow of water, leading to pressure pulsations (Favrel et al., 2018).

To date, numerous measures have been suggested to ameliorate flow conditions in the draft tube and mitigate the formation of vortex ropes (Muhirwa et al., 2020). Common measures include implementing a baffle or fin structure (Zhou et al., 2019), improving the shape of the runner cone (Li et al., 2021; Qian et al., 2012), optimizing the geometry of the draft tube (Arispe et al., 2018; Favrel et al., 2021; Shrestha & Choi, 2021; Zhou et al., 2021, 2023), introducing high pressure water jet (Bosioc et al., 2012; Foroutan & Yavuzkurt, 2014) or air into the low-pressure zone inside the draft tube, or a combination of these methods(Zhu et al., 2021). The SST k-ω turbulent model and the homogeneous mixture assumption are often used to conduct studies on the effectiveness of different methods in mitigating pressure fluctuations in the draft tube of turbine units. These studies were conducted using computational fluid dynamics (CFD) numerical simulation methods (Rajan & Cimbala, 2016), in conjunction with experimental data obtained from prototype testing (Ji et al., 2022). It has been found that injecting air into the draft tube is one of effective ways to alleviate pressure fluctuations in Francis turbine unit (Zhu et al., 2021). For example, Qian et al.(2007) utilized the RNG k-ε turbulence model to inject air through a Francis turbine's spindle hole at rates of 0.25%, 0.50%, and 0.75% of the discharge. The study found that an air-water ratio of 0.50% was effective in reducing the amplitude of the turbine's low-frequency pressure pulsations. Similarly, Yu et al. (2015, 2020) conducted numerical simulations with a wider range of air admission rates ranging from 0.5% to 4.0% of water discharge at the inlet plane, which revealed that the vortex rope diameter increased and the pressure fluctuation amplitude slightly increased at a ratio of 0.5%. However, when the air-water ratio reached 4.0%, the amplitude of pressure fluctuation was significantly reduced, and there was no significant dominant frequency of pressure fluctuation. Zhu et al. (2021) developed various strategies to eliminate the vortex low-pressure zone in the draft tube of a Francis turbine. The study found that using only air admission from the runner cone could make the pressure distribution in the draft tube more uniform. At higher air admission flow rates, this approach transformed the spiral vortex rope into a cylindrical vortex rope, which could not come into direct contact with the draft tube wall, thereby reducing the amplitude of pressure fluctuations in the turbine units. In order to analyze whether the air admission causes more energy loss to the turbine, the entropy production theory is used to analyze the entropy production of each component of the turbine before and after air admission. This method has been applied to analyze the S-characteristics of the pump turbine (Gong et al., 2017), or to analyze the energy loss of the Francis turbine operating at partial load conditions (Yu et al., 2021b). Due to computational resource constraints and challenges in two-phase flow calculations, there is relatively little research on the use of air admission measures to reduce the pressure fluctuations in the draft tube, and the previous research is mainly focused on the Francis turbine units (Ji et al., 2022). There is still a lack of numerical and experimental data for propeller hydro-turbines.

In this study, two different air admission methods were investigated by CFD simulation to alleviate the vortex rope in a propeller hydro-turbine draft tube. The degree of suppressing the vortex rope oscillation with these two methods was evaluated. Using the entropy production theory to determine the entropy production on each component of the turbine, the energy loss due to the air admission measure was quantified, and an attempt was made to clarify the cause of the additional energy loss due

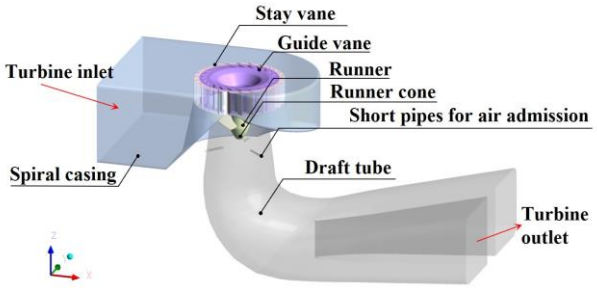

Fig. 1 3D flow passage of the hydro-turbine

Table 1 Specification of the hydro-turbine

Structural parameters	Value	Performance parameters	Value
Stay vane number	24	Unit rotating speed	128.7 r/min
Guide vane number	24	Unit discharge	1.603 m^3/s
Runner blade number	5	Design efficiency	92.50%
Runner diameter, D	3.33 m	Specific speed, n_s	492.4

to air injecting in the draft tube. The pressure fluctuations were analyzed using the fast Fourier transform, with particular emphasis on the effects of the two air admission methods under a partial load condition. The main novelties of this paper are that it analyzes the effect of air admission measures using entropy production theory and it concludes that air stagnation in the draft tube elbow is responsible for the reduction in hydraulic efficiency. This study also enriches the research data on the effect of air admission on mitigating pressure fluctuations in the draft tube of propeller hydro-turbine units. This study can provide additional solution ideas and data for balancing unit efficiency and stability when scheduling units using an AGC strategy.

2. NUMERICAL MODEL AND METHODOLOGY

2.1 Propeller Hydro-turbine Model and Structure for Air Admission

The propeller hydro-turbine is used as the subject of this study. This type of hydro-turbine flow passage consists of five components including spiral casing, guide vanes, stay vanes, runner, and draft tube, as well as three short pipes for air admission installed in the draft tube wall. A hole is left in the center of the runner cone for air admission. The complete three-dimensional flow passage of the hydro-turbine is shown in Fig. 1. The main structural parameters and the main hydraulic performance parameters are given in Table 1.

It is worth mentioning that the specific speed, n_s, is an important similar parameter that can reflect the operating characteristics of the hydro-turbine and is defined as follows:

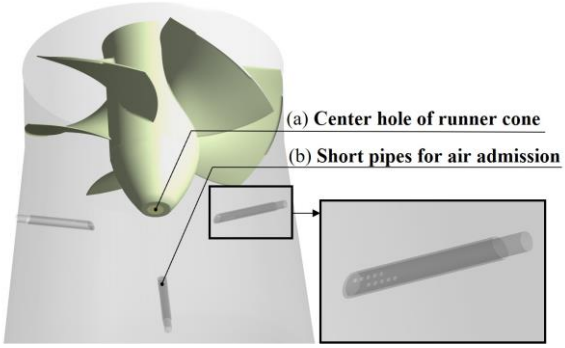

Fig. 2 Two structures for air admission (a) Center hole of runner cone, (b)Short pipes for air admission

$$n_s = \frac{n\sqrt{P}}{H^{5/4}} \tag{1}$$

where n is the rotating speed of the runner (166.7r/min), P is the rated output of the hydro-turbine (13MW) and H is the rated head (18.6m).

The prototype hydro-turbine was equipped with two different structures for air admission as shown in Fig. 2. Figure 2(a) shows the scheme of opening a hole in the center of the runner cone and using this center hole to inject air. This center hole is 100 mm in diameter. Figure 2(b) shows the scheme of using three short pipes with open holes to inject air into the draft tube cone. There are 10 holes on each of the three short pipes for air admission, arranged on the left and right sides of the end of the short pipes, with 5 holes on each side. The diameter of the holes is 25 mm. The short pipes were fixed inside the draft tube of the prototype turbine and were not removable. The supplemental air can enter the low-pressure zone in the draft tube cone through the open holes in both schemes.

2.2 Grid Independence Verification

Due to the complex structure of the hydro-turbine, the entire flow passage was discrete into five parts with different mesh sizes and mesh types, and then the mesh of each part was generated independently. Tetrahedral unstructured grids were used for the spiral casing, runner, and draft tube, and hexahedral structured grids were used for the stay vane and guide vane. Numerical simulation accuracy and the cost were balanced by evaluating the mesh size around the runner, the guide vane, the short pipes for air admission, and the runner cone. Figure 3 shows the meshes of each hydro-turbine component.

The efficiency and power of the unit were selected as the indices for the grid sensitivity analysis. Six mesh models with different grid numbers were designed for numerical simulation under low flow conditions (GVO = 32°). When the number of grid nodes is more than 3 million, the fluctuation of efficiency is less than 0.2% and the fluctuation of power is less than 0.1kW, as shown in Fig. 4. The calculation results of efficiency and power are almost unaffected by the number of grids, which is considered to be the convergence of the calculation. In this study, there are 3.7 million grid nodes in the computational domain, which can meet the numerical simulation accuracy requirement. The final grid nodes number of the selected mesh model is shown in Table 2.

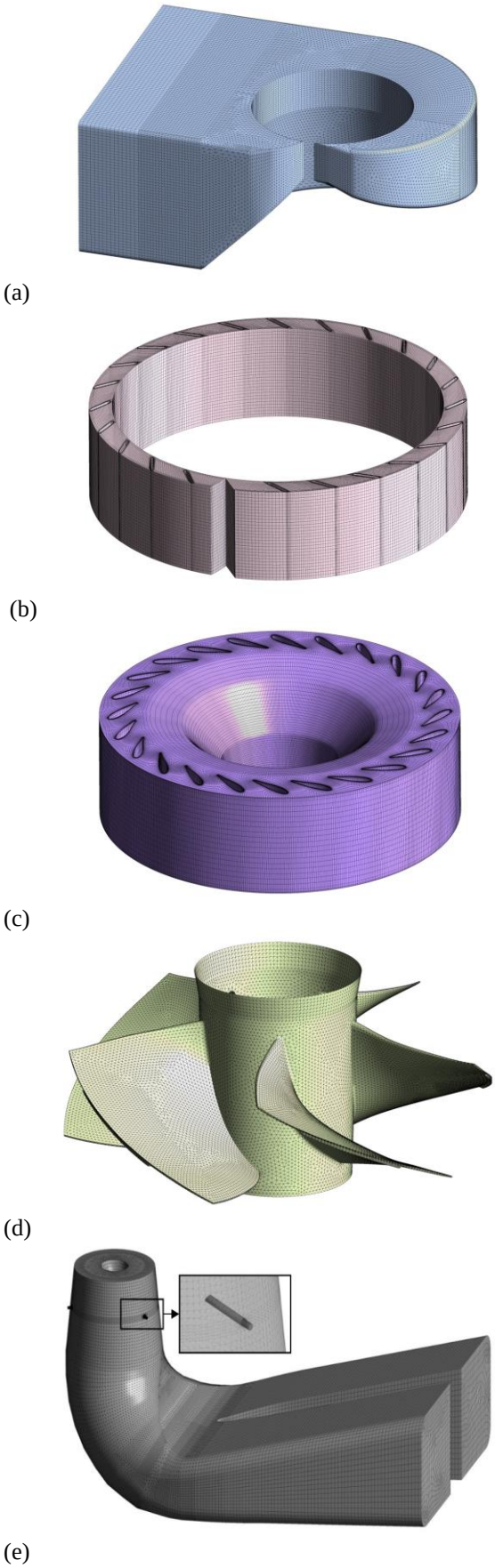

Fig. 3 Mesh of hydro-turbine (a) Spiral casing grids, (b) Stay vane grids, (c) Guide vane grids, (d) Runner grids, (e) Draft tube grids (including short pipes for air admission)

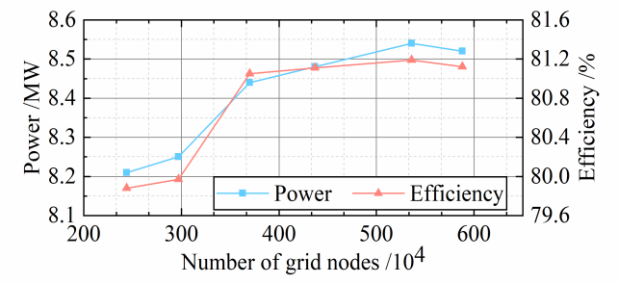

Fig. 4 Grid sensitivity analysis

Table 2 Number of nodes of the propeller turbine grid

Component	Spiral casing	Stay vane	Guide vane
Nodes ($\times 10^6$)	0.27	1.06	0.80
Component	Runner	Draft tube	Total
Nodes ($\times 10^6$)	1.05	0.52	3.70

2.3 Turbulence Model and Governing Equations

Based on the finite volume method, the commercial computational fluid dynamics (CFD) software ANSYS CFX 18.0 was used to solve the incompressible three-dimensional unsteady turbulent flow inside the hydro-turbine. The shear stress transport (SST) k-ω turbulence model based on the Reynolds averaged Navier-Stokes (RANS) equations was used when no air was injected into the hydro-turbine. This turbulence model can produce simulation results with less error when simulating complex internal flows, and it is less sensitive to free stream conditions. This model uses turbulent kinetic energy k and dissipation rate ω to calculate the turbulent eddy viscosity μ_t. The governing equations are shown in Eqs. (2)~ (3)(Menter, 1993).

$$\frac{\partial}{\partial t}(\rho_w k)+\frac{\partial}{\partial x_i}(\rho_w k u_i)=\frac{\partial}{\partial x_j}[\left(\mu+\frac{\mu_t}{\sigma_k}\right)\frac{\partial k}{\partial x_j}]+P-\beta^*\rho_w\omega k \tag{2}$$

$$\frac{\partial}{\partial t}(\rho_w\omega)+\frac{\partial}{\partial x_j}(\rho_w\omega u_j)=\frac{\partial}{\partial x_j}\left((\mu+\sigma_\omega\mu_t)\frac{\partial\omega}{\partial x_j}\right)+2(1-F_1)\frac{\rho_w}{\sigma_{\omega 2}\omega}\frac{\partial k}{\partial x_j}\frac{\partial\omega}{\partial x_j}+\frac{\rho_w\gamma}{\mu_t}P-\beta\rho_w\omega^2 \tag{3}$$

where ρ_w represents the density of water, μ represents the dynamic viscosity, P represents the production term, σ_k, σ_ω, β and β^* are the model constants.

In the case of air admission measures, the two-phase gas-liquid flow inside the hydro-turbine was solved by using a model based on the homogeneous mixture assumption. The mixture density ρ and the viscosity μ can be described by Eqs. (4)~(5).

$$\rho=\rho_v\alpha_v+\rho_l(1-\alpha_v) \tag{4}$$

$$\mu=\mu_v\alpha_v+\mu_l(1-\alpha_v) \tag{5}$$

where v and l are subscripts for the vapor and liquid, ρ represents the density of the vapor-liquid mixture, α is the volume fraction of the vapor.

If the velocity slip between the vapor and the liquid is neglected, the basic governing equation for the mixture can be described by Eqs. (6)~(7).

$$\frac{\partial \rho}{\partial t}+\frac{\partial(\rho u_j)}{\partial x_j}=0 \tag{6}$$

$$\frac{\partial(\rho u_i)}{\partial t}+\frac{\partial(\rho u_i u_j)}{\partial x_j}=-\frac{\partial p}{\partial x_i}+\frac{\partial}{\partial x_j}(\mu\frac{\partial u_i}{\partial x_j}) \tag{7}$$

2.4 Numerical Scheme and Setting

Numerical simulations were performed for 15 turbine operating conditions and their corresponding air admission conditions between 0.8*Q* and 1.0*Q* (*Q* for rated discharge) by adjusting the guide vane opening (GVO, between 31° and 45°). The runner domain was set as a rotating domain, while the rest of the parts were set as stationary domains. The rotor-stator interfaces were used to exchange data between the rotating and stationary domains, and the general grid interfaces were used to exchange data between the other domains. All solid surfaces of the entire flow passage were set to no-slip conditions.

For the numerical simulations in the transient frame, the results of the steady case were used as the initial values. To determine the time step in the unsteady calculation, the independence of the time step was verified using the pressure fluctuation data from the monitoring point on the head cover.

The time step was set to 0.0018s, 0.0024s, 0.0036s, and 0.0072s, corresponding to 200, 150, 100, and 50 steps for each revolution of the runner, respectively. The data were subjected to an FFT, then the pressure fluctuation and the frequency spectra at this monitoring point were obtained, as shown in Fig. 5. When the time step was set to 0.0018s or 0.0024s, the amplitude at the dominant frequency differs by 0.2%, which was considered computational convergence. To balance computational resources and accuracy, it was finally decided to set the time step to 1/150 of the rotation period of the runner (0.0024s), which means that 1 step was calculated for every 2.4° rotation of the runner.

The convergence criterion root mean square (RMS) was set as 10^{-5}, and all residuals need to be less than 10^{-3}. The total calculation time of the unsteady simulation was set to 10.8s. To reduce the influence of initial values on

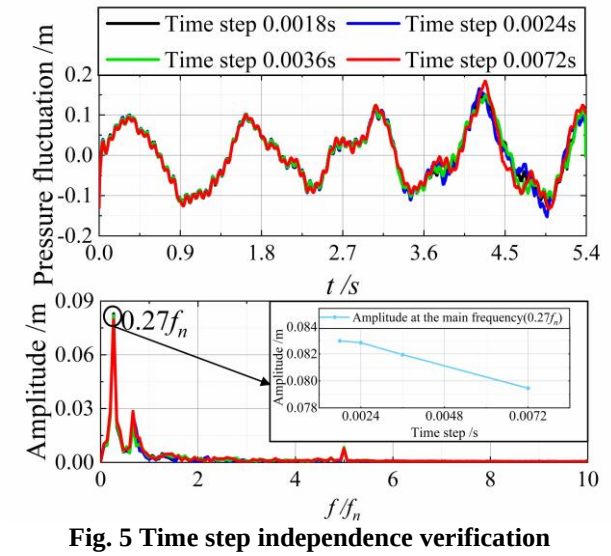

Fig. 5 Time step independence verification

Table 3 Numerical simulation parameter settings

Turbulence model	RANS *SST k-ω*	
Multiphase flow model	Mixture Model Homogeneous Flow Model	
Time step	0.0024 s	
Boundary pressure	Spiral casing inlet	0.248 MPa
	Draft tube outlet	0.078 MPa
Type of boundary for air admission	Short pipes	Mass flow rate inlet
	Runner cone center hole	

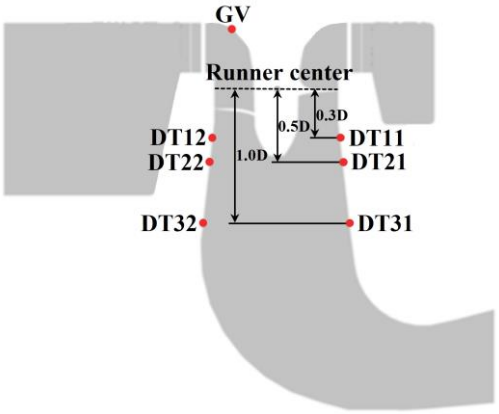

Fig. 6 Monitoring points in the draft tube

the unsteady calculation, the data of 7.2-10.8s were selected for analysis and processing in order to better meet the requirements of calculation accuracy. The main parameters in the numerical simulation are listed in Table 3.

2.5 Monitoring Points

As shown in Fig. 6, a total of seven pressure monitoring points were set to monitor pressure fluctuations in the internal flow of the propeller turbine draft tube. Since the vortex rope appears mainly in the draft tube cone, three sets of pressure monitoring points were set up inside the draft tube cone, at distances of 0.3*D*, 0.5*D*, and 1.0*D* from the runner center. Considering that the draft tube is not symmetrical in the flow direction, monitoring points were set up at both the left and right sides of the draft tube wall. Since the pressure fluctuation monitoring point of the prototype turbine was set only on the head cover, a monitoring point was set at the same position on the numerical model head cover to compare the numerical simulation data with the experimental data.

3. RESULTS AND DISCUSSIONS

3.1 Numerical Simulation Verification

This section presents the results of a numerical simulation test performed under low flow conditions that produced an observable pressure pulsation phenomenon. The experimental data of the prototype was used as a benchmark for comparison. The experiment was performed with a head of 16.5m and a guide vane opening

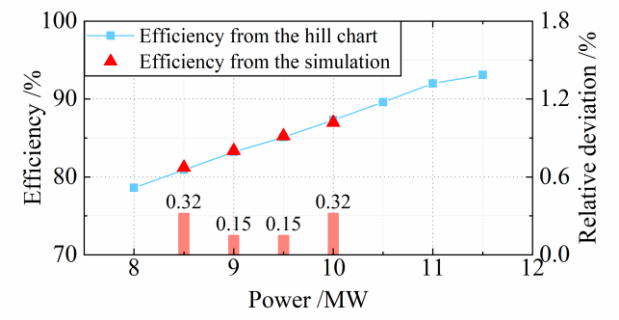

Fig. 7 Efficiency - Power under low flow conditions

adjusted to achieve a turbine power of 8.5MW (GVO = 32°) to ensure consistency between the simulation and prototype conditions. A Monitoring Point GV was set on the head cover of the hydro-turbine in the numerical simulation model, and the simulation was conducted in unsteady condition.

Figure 7 presents a comparison between the efficiency of the hydro-turbine under low flow conditions obtained by numerical simulation and the characteristic curve derived from experimental data on the hill chart. In the numerical simulation, the efficiency of the hydro-turbine is 81.22% (8.5 MW), 83.35% (9.0 MW), 85.25% (9.5 MW) and 86.98% (10.0 MW) when the head was set to 16.5 m. The experimental efficiency obtained from the hill chart refers to the product of the hydraulic efficiency η_h and the volumetric efficiency η_v . And that the mechanical efficiency η_m has been excluded. Therefore, the physical meanings of the efficiencies in Fig. 7 are consistent with each other. The experimental hydraulic efficiency of the turbine is calculated by the following Eqs. (8)~(9).

$$\eta_h = \frac{H-\Delta H}{H} = 1 - \frac{\Delta H}{H} \tag{8}$$

$$\eta_v = \frac{Q-\Delta Q}{Q} = 1 - \frac{\Delta Q}{Q} \tag{9}$$

where H is head, ΔH is hydraulic loss, Q is flow, and ΔQ is leaked flow.

The analysis shows that the maximum relative deviation of efficiency in the numerical simulation is 0.32%, while the minimum is as low as 0.15%, under the investigated conditions. This indicates that the numerical model of pressure fluctuation of the propeller hydro-turbine constructed in this study has a sufficient calculation accuracy.

The fast Fourier transform was utilized to analyze the dominant frequency and amplitude of the pressure fluctuation (Cao et al., 2022). The pressure fluctuation values at each monitoring point were subtracted from the average value and converted into head values in meters. The results of the comparison are shown in Fig. 8. It is apparent from the frequency spectra that the dominant frequency of the pressure fluctuation obtained from the simulation matched with the experimental dominant frequency of $0.27f_n$ (f_n for the rotating frequency of the runner). The simulation results indicated that the amplitude of the pressure fluctuation corresponding to the dominant frequency was 0.096 m, while the experiment

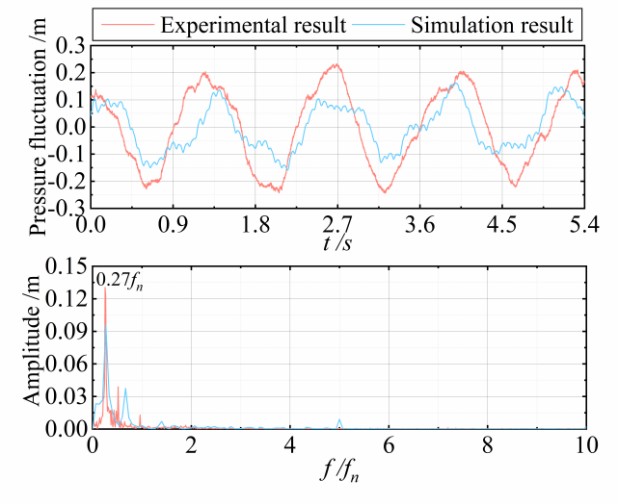

Fig. 8 Verification of simulation results against experimental results

showed an amplitude of 0.131m. The deviation between the two was within an acceptable range. The amplitude error was primarily due to the position error of the monitoring points during the experiment and simulation, experimental measurement errors, and numerical errors.

3.2 Selection of the Air Flow Rate

In order to suppress vortex rope formation in the draft tube of hydro-turbines, it is necessary to choose the suitable air-water ratio when using two different methods of air admission. Under the partial load condition, characterized by a guide vane opening of 32° and a flow rate of $0.85Q$ for the hydro-turbine, significant low-frequency pressure fluctuations occurred in the draft tube, resulting in the observation of a significant vortex rope. The vortex rope region has high swirling strength, so the Q-criterion can be used for vortex identification (Zhan et al., 2020).

When using the short pipes with open holes to inject air, the air flow rate was set to $0.01Q$, $0.02Q$, $0.03Q$, $0.04Q$, $0.05Q$, $0.06Q$, $0.07Q$, $0.08Q$, and the supplemental air was evenly distributed at the inlet of the three short pipes, and the boundary of the air inlet was set as mass flow rate inlet. The simulation results demonstrated that the vortex rope below three short pipes can be destroyed when the flow rate of air admission reached $0.05Q$. Additionally, the air was able to enter the low-pressure zone of the lower half vortex rope more smoothly, as shown in Fig. 9. Therefore, an air flow rate of $0.05Q$ was determined as optional for eliminating the vortex rope using short pipes under partial load conditions.

When using the runner cone center hole to inject air, the air flow rate was set to $0.011Q$, $0.012Q$, $0.013Q$, $0.014Q$, $0.015Q$, $0.016Q$, $0.017Q$, $0.018Q$. The reason for setting the interval of the air flow rate smaller is that the center hole is closer to the vortex rope and the air can go directly into the region with a large pressure gradient. Therefore, with the same flow rate, using the center hole to eliminate the vortex rope effect may be better, and it is not appropriate to use an excessive air flow rate. The numerical simulation results showed that the vortex rope

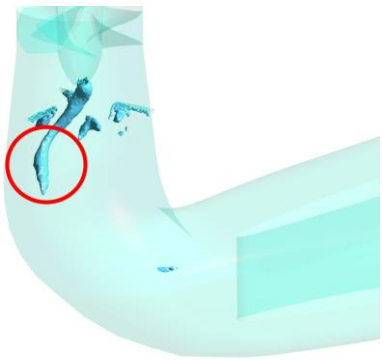

(a)

(b)

Fig. 9 Shape of vortex rope in the short pipe scheme. (a)GVO32° 0.04*Q*, (b)GVO32° 0.05*Q*

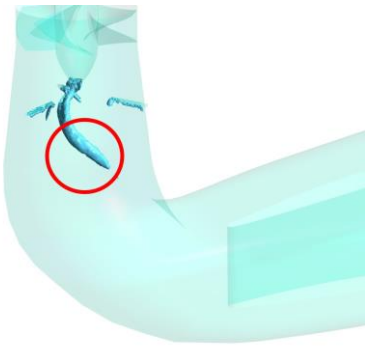

(a)

(b)

Fig. 10 shape of vortex rope in the runner cone center hole scheme (a)GVO32° 0.013*Q*, (b)GVO32° 0.014*Q*

was destroyed when the air flow rate reached 0.014*Q*, and the optimal effect of eliminating the vortex rope was achieved, as shown in Fig 10. Therefore, under partial load conditions, the flow rate of air admission using the center hole was chosen as 0.014*Q*.

3.3 Vortex Rope and Pressure Distribution in the Draft Tube

This section mainly discusses the morphology of vortex ropes and the pressure distribution on the middle cross-section of the draft tube under three different air admission conditions. When hydro-turbine operated under partial load conditions, the low-frequency pressure pulsations generated in the draft tube were mainly caused by vortex ropes.

As shown in Fig. 11, compared with the condition without air admission, whether using short pipes or a center hole of the draft cone to inject air, the length of the vortex rope significantly decreased and the diameter also reduced if the air flow rate was appropriate. However, new vortices may generate around the short pipes.

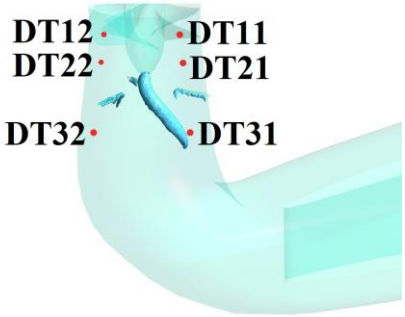

(a)

(b)

(c)

Fig. 11 Morphology of vortex rope for partial load condition (GVO 32°, 0.85*Q*) (a)No air injection, (b)Injecting air by short pipes, (c)Injecting air by runner cone center hole

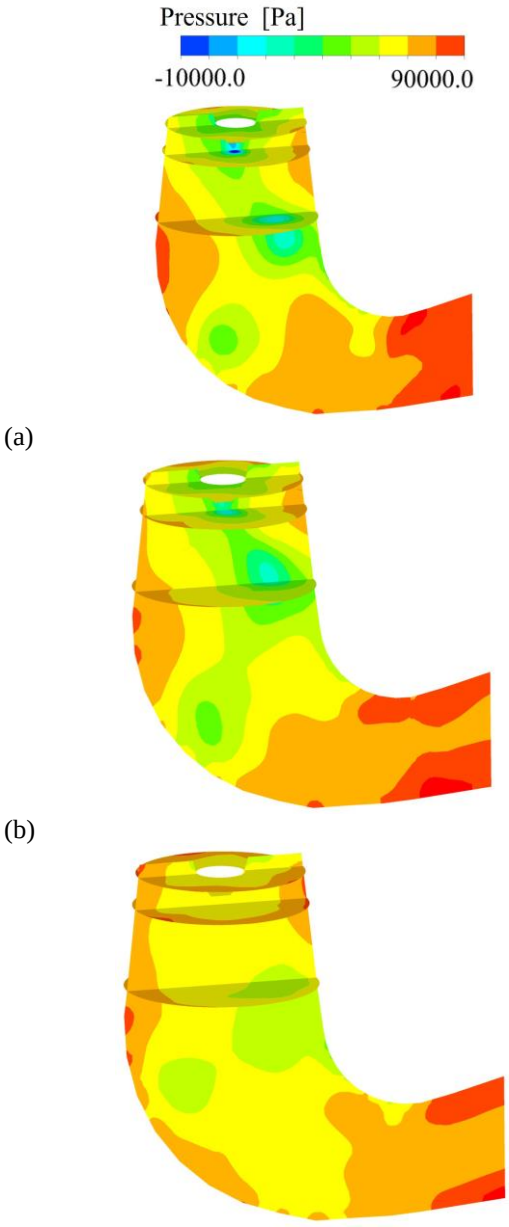

Fig. 12 Pressure distribution in the draft tube for partial load condition (GVO 32°, 0.85*Q*) (a)No air injection, (b)Injecting air by short pipes, (c)Injecting air by runner cone center hole

Figure 12 shows more visually that injecting air into the draft tube results in a more uniform pressure distribution. And it can reduce the amplitude of alternating pressure on the draft tube wall caused by vortex ropes.

3.4 Energy Production and Efficiency Loss Analysis

At partial load conditions, although injecting air into the draft tube can make the pressure distribution more uniform, it can also result in hydraulic losses. Therefore, it is necessary to analyze the hydro-turbine operating conditions under air admission using the vorticity transport equation and entropy production theory, and it is important to reveal the mechanism between vortex ropes and energy loss. The entropy production theory helps to analyze the energy losses in the entire flow path of the hydro-turbine.

While neglecting the viscous diffusion term and baroclinic torque term, the vorticity transport equation is shown as Eq. (10).

$$\frac{D\vec{\omega}}{Dt} = (\vec{\omega}\cdot\nabla)\vec{V} - \vec{\omega}(\nabla\cdot\vec{V}) \tag{10}$$

where $\vec{\omega}$ represents the relative vorticity, $\vec{V}$ represents the time-averaged relative velocity.

From the perspective of the second law of thermodynamics, the energy dissipation process inside the hydro-turbine is irreversible, and the increase in entropy is inevitable (Yu et al., 2021b). In the Reynolds time-averaging method, time-averaged entropy production can be divided into the time-averaged part and fluctuating part, as shown in Eq. (11).

$$S = S_{\bar{D}}^{'''} + S_{D'}^{'''} \tag{11}$$

where $S_{\bar{D}}^{'''}$ represents the direct dissipation, $S_{D'}^{'''}$ represents the indirect dissipation. In the internal flow process of a hydro-turbine, due to the turbulence effect, the entropy production rate induced by the fluctuating velocity $S_{D'}^{'''}$ dominates. Therefore, this term can be used as an indicator to analyze the energy dissipation process (Zhou et al., 2022). The generalized formula for calculating indirect dissipation can be written as Eq. (12).

$$\begin{aligned} S_{D'}^{'''} = \frac{2\mu}{T}\left[\left(\frac{\partial u'}{\partial x}\right)^2 + \left(\frac{\partial v'}{\partial y}\right)^2 + \left(\frac{\partial w'}{\partial z}\right)^2\right] \\ + \frac{\mu}{T}[\left(\frac{\partial u'}{\partial y} + \frac{\partial v'}{\partial x}\right)^2 \\ + \left(\frac{\partial w'}{\partial x} + \frac{\partial u'}{\partial z}\right)^2 \\ + \left(\frac{\partial v'}{\partial z} + \frac{\partial w'}{\partial y}\right)^2] \end{aligned} \tag{12}$$

Where u', v', w' are fluctuating velocity components.

Since the SST k-ω turbulence model cannot obtain the velocity fluctuation component directly, a new solution method is needed to obtain the entropy production due to velocity fluctuation. The local entropy generation rate due to velocity fluctuations is thought to be closely related to the turbulent mode of ε or ω, thus, the method proposed by Kock (Kock & Herwig, 2004) is usually used to determined $S_{D'}^{'''}$. The expression for $S_{D'}^{'''}$ is shown in Eq. (13).

$$S_{D'}^{'''} = \beta\frac{\rho\omega k}{T}, \beta = 0.09 \tag{13}$$

Where β is an empirical constant.

The value of β is given by Menter (Menter, 1994), the scholar who developed the SST $k-\omega$ turbulence model.

For a certain part of the hydro-turbine, the entropy induced by the fluctuating velocity can be obtained by calculating the volume integral in Eq. (14).

$$S_{D'} = \int S_{D'}^{'''} dV \tag{14}$$

The results can be used to measure the magnitude of energy losses on various parts of the hydro-turbine.

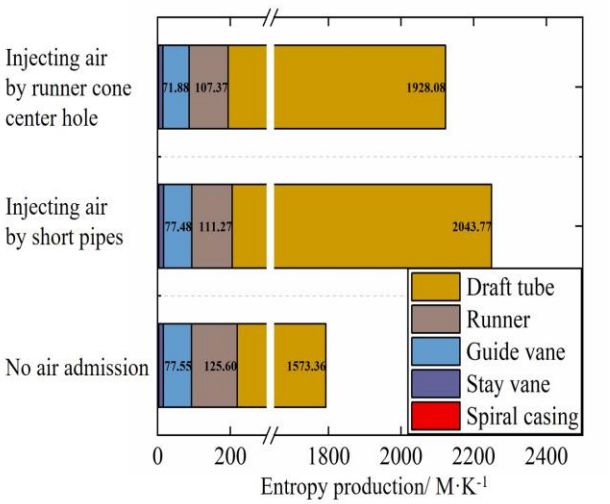

Fig. 13 Entropy induced by the fluctuating velocity of the hydro-turbine components (GVO32°)

In this study, the energy losses on various parts of the hydro-turbine were compared under two different air admission conditions and a no air condition. As shown in Fig. 13, these losses were described by the volume integral of the indirect dissipation term $S_{D'}^{\prime\prime\prime}$ for each component, denoted as $S_{D'}$. It was found that the majority of the energy losses occurred in the draft tube. The air admission measures significantly increased the entropy induced by the fluctuating velocity in the draft tube. However, it also reduced the energy losses in other components.

To investigate the impact of the increased entropy, the entropy production rate distribution is presented in Fig. 14. It is found that injecting air into the draft tube results in an increase in energy dissipation during the flow process. The losses are particularly significant when the water flows through the air outlet of the air admission structure in the hydro-turbine. The water carries the air downstream to the draft tube, and the air stays at the draft tube elbow, obstructing the flow of water and causing efficiency losses.

To quantitatively compare the efficiency loss caused by the air admission, the total pressure on the interfaces between each part of the hydro-turbine was used to calculate the efficiency loss. The calculation formula is shown in Eq. (15).

$$\eta_i = \frac{p_{i-in} - p_{i-out}}{p_{loss}} \times 100\% \tag{15}$$

This equation is applicable for calculating the efficiency loss on hydro-turbine parts other than the runner. Here, p_{loss} represents the total pressure drop between the spiral casing inlet and the draft tube outlet. When calculating the efficiency loss on the runner, Eq. (16) can be used as a substitute.

$$\eta_i = \frac{p_{i-in} - p_{i-out} - \tau\omega/Q_{in}}{p_{loss}} \times 100\% \tag{16}$$

where τ denotes the torque of the runner, ω denotes the angular rotation speed of the runner, and Q_{in} denotes the volume flow rate at the spiral casing inlet.

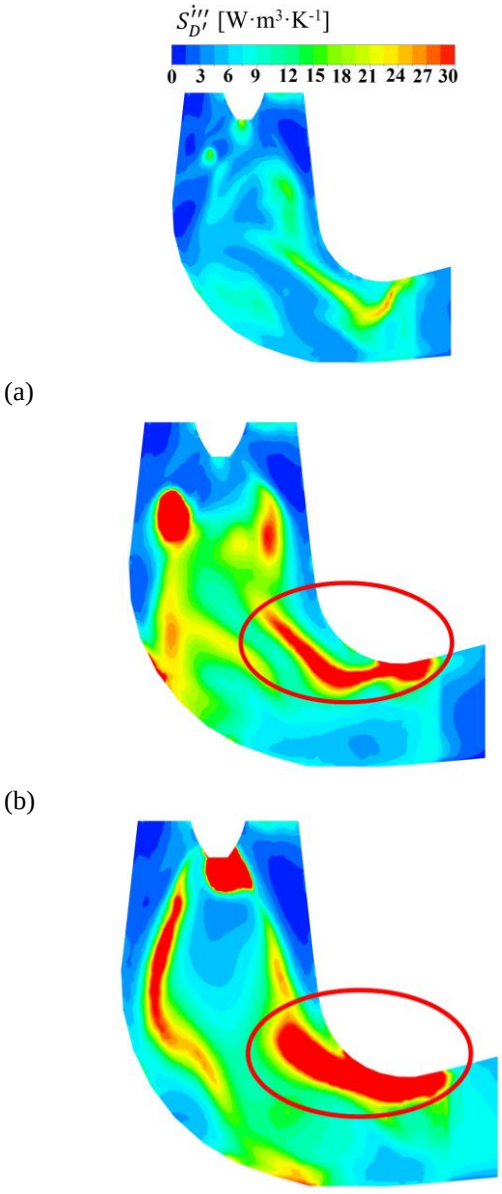

Fig. 14 Distribution of entropy production rate on the cross-section of the draft tube (GVO32°) (a)No air injection, (b)Injecting air by short pipes, (c)Injecting air by runner cone center hole

It was found that the air admission measures will increase the efficiency loss of the hydro-turbine, and the increased efficiency loss is within the range of 3% to 5%, as shown in Fig.15.

3.5 Pressure Fluctuations Before and After Air Admission

In order to clarify whether the effects of reducing pressure fluctuations by using the two measures for air admission were good or not, the partial load condition with guide vane opening of 32° (0.85Q) was selected to analyze, and the iso-surface of vorticity was drawn, the pressure pulsation in unsteady conditions was obtained, as shown in Fig. 16.

The calculation results indicate that although injecting air by short pipes or runner cone center hole can reduce the low-frequency pressure pulsation caused by the

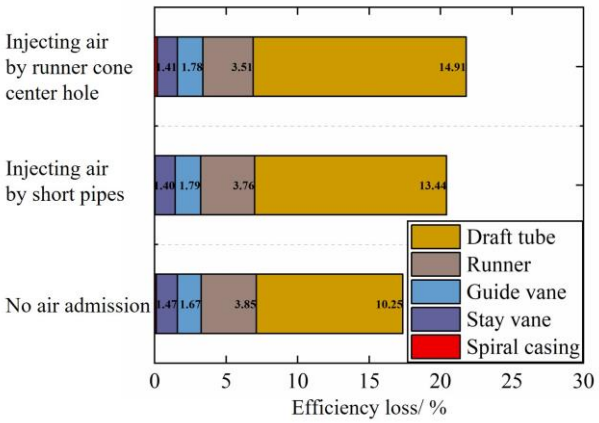

Fig. 15 Efficiency losses of the hydro-turbine components (GVO32°)

vortex rope, especially the amplitude corresponding to the dominant frequency, the robustness of the two schemes is different. Injecting air through the runner cone center hole has less robustness in reducing the amplitude of pressure fluctuation. As shown in Fig. 16(c), at the monitoring point DT31 in the draft tube cone, air admission increased the pressure pulsation. At the same time, it was observed that the shape of the vortex rope in the draft tube was extremely irregular, indicating that the flow state was more chaotic. On the contrary, the scheme of injecting air through short pipes can stably reduce the amplitude of pressure pulsation at almost each monitoring point and destroy the main body of the vortex rope.

As shown in Fig. 17, the dominant and partial secondary frequencies of the pressure fluctuation have been marked in the frequency spectra. In this partial load

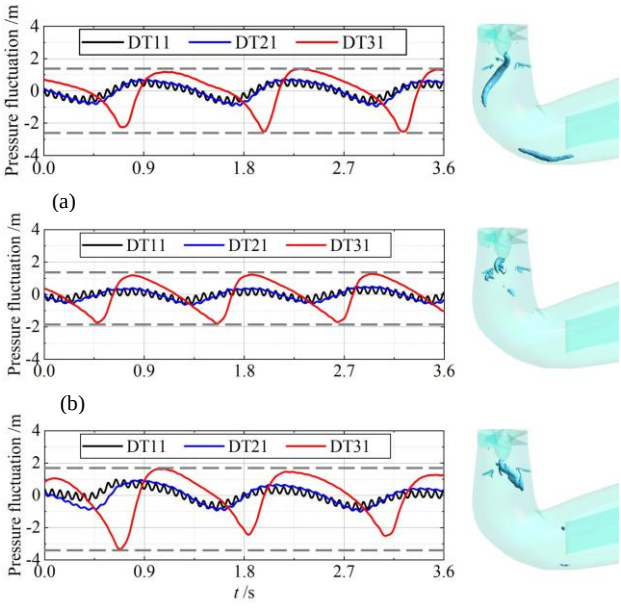

Fig. 16 Vortex ropes and pressure fluctuations of each monitoring point under the part-load condition (GVO32°) (a)No air injection, (b)Injecting air by short pipes, (c)Injecting air by runner cone center hole

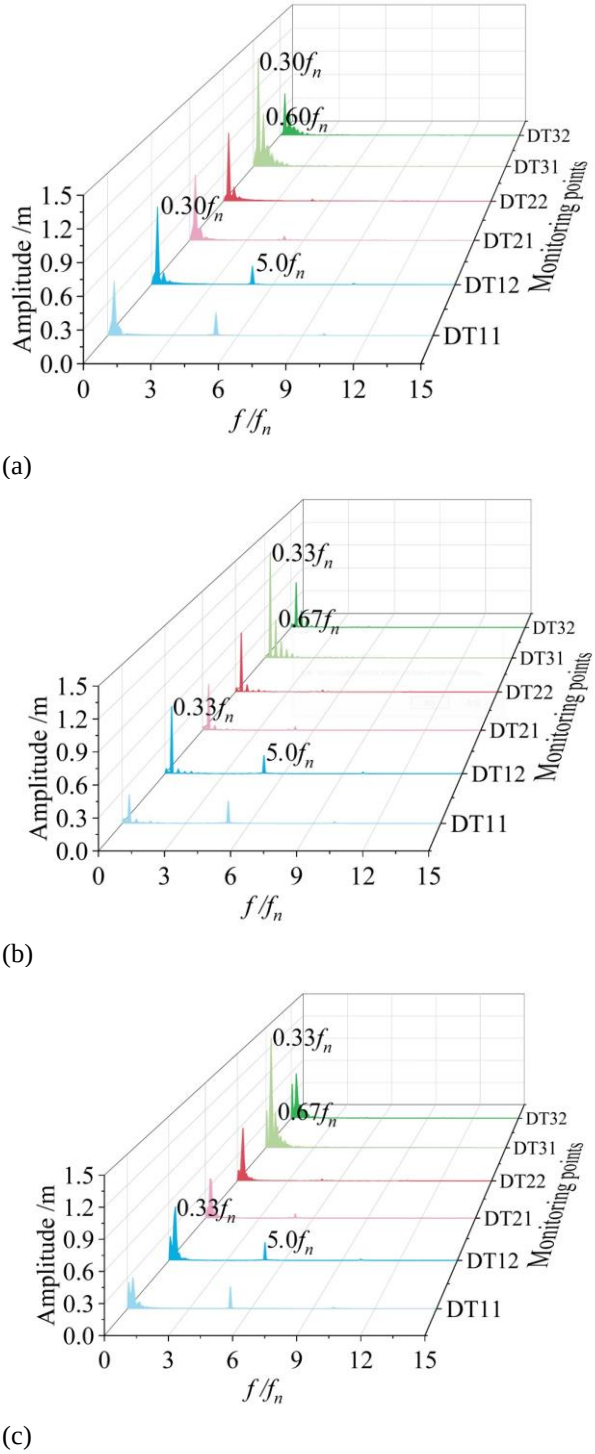

Fig. 17 Frequency spectra of each monitoring point under the typical part-load condition (GVO32°) (a)No air injection, (b)Injecting air by short pipes, (c)Injecting air by runner cone center hole

condition, the dominant frequencies were found to lie within the range of $0.27f_n$ to $0.33f_n$, which correspond to low-frequency, high-amplitude vibrations induced by the vortex rope. The frequency of $5.0f_n$ corresponds to the vibrations resulting from the passage of the runner blades. It was observed that the use of short pipes for air admission to eliminate the pressure pulsation in low-frequency was more effective than injecting air through the runner cone center hole as a solution.

Pressure at each monitoring point

This section primarily analyzed the pressure fluctuation intensity at six monitoring points on the draft tube wall. Numerical simulation calculations were performed for conditions with guide vane openings ranging from 31° to 36°, including cases without air admission, and with air admission through the short pipes or the runner cone center hole.

Air admission was performed for a duration of 10.8s in unsteady condition, and pressure pulsation data from the last 3.6s were selected for analysis to avoid convergence problems that may be caused by the initial state. This is because the initial flow field affects the calculation of the pressure pulsations for a small period of time from just entering the unsteady calculation, but this effect diminishes with time. Therefore choosing data before the end of the calculation for analysis is the preferred choice. Moreover, the pressure fluctuation data obtained within 3.6s can satisfy the requirement of FFT on the amount of data. The pulsation amplitude data of the alternating pressure at a monitoring point within 10 hydro-turbine revolutions (3.6s) was calculated using FFT and defined as the pressure fluctuation intensity at this monitoring point, with the unit in meter, as shown in Fig. 18. It can be observed that as the guide vane opening increased, the amplitude of pressure fluctuation gradually decreased to a lower level.

Referring to the location of the monitoring points shown in Fig. 6, DT11 and DT12 are located to the right and left of the draft tube wall, respectively. It is found that when the monitoring point is close to the runner center, the pressure fluctuation amplitude on the right side (DT11) is smaller than that on the left side (DT12). On the contrary, when the monitoring point is far from the runner center, the pressure fluctuation amplitude on the right side (DT31) is greater than that on the left side (DT32). This is caused by the asymmetry of the draft tube. On the same left side, the pressure fluctuation close to the runner (DT12) is greater. On the same right side, the pressure fluctuation far from the runner (DT31) is greater. This is because the vortex rope can have more contact with these two positions, resulting in greater pressure gradients and larger pressure fluctuations on the draft tube wall.

The calculation results showed that the pressure fluctuation amplitudes at each monitoring point, except for conditions at monitoring points DT32 and certain conditions at monitoring points DT31, are reduced to some extent. When the guide vane opening is smaller than 33 °, injecting air through the runner cone can reduce pressure fluctuation intensity to a greater extent. When the guide vane opening reaches 34° or greater, injecting air through short pipes can achieve better results. For the reason of pressure fluctuation amplitude increasing at monitoring point DT32 after air admission in conditions with a small guide vane opening, it may be the air admission changes the shape and position of the vortex rope, causing the remaining vortex rope to be closer to this area and increasing the pressure gradient and the pressure fluctuation intensity near DT32. The above analysis indicates that both air admission measures have an effect in alleviating pressure pulsations in the draft tube.

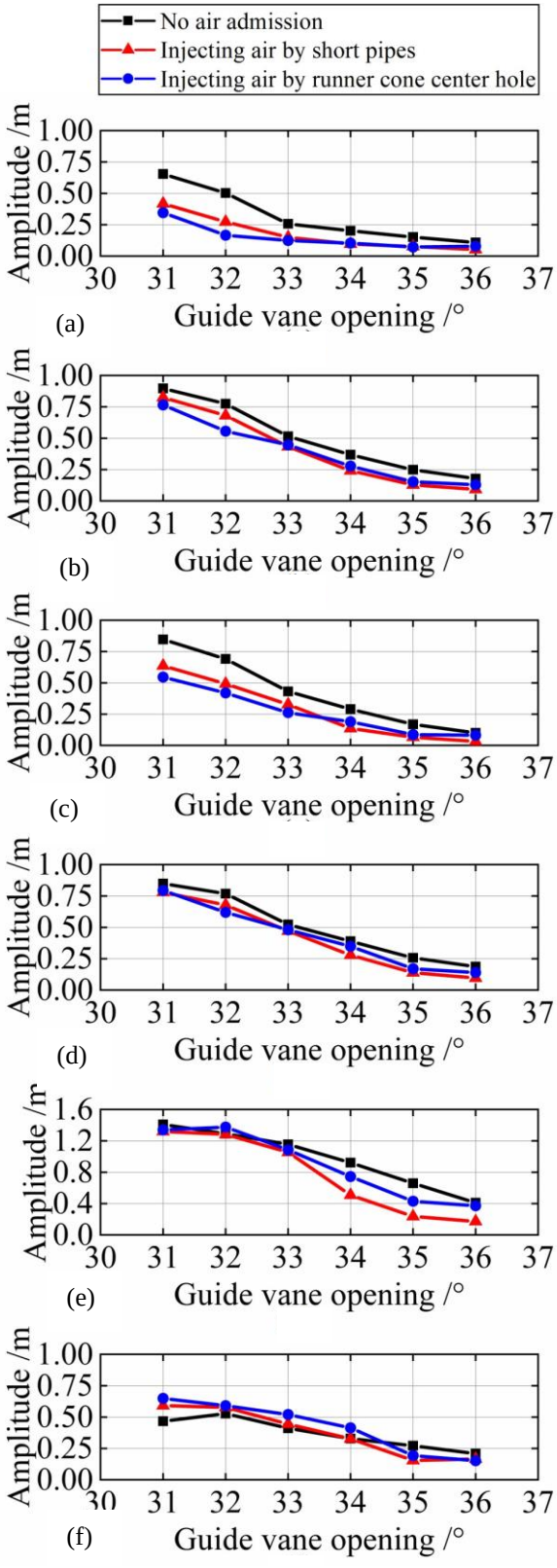

Fig. 18 Amplitude at the dominant frequency of the pressure fluctuation at monitoring points (a)DT11, (b)DT12, (c)DT21, (d)DT22, (e)DT31, (f)DT32

The average data of the amplitudes in the dominant frequency of six monitoring points in the draft tube were selected to provide a simple quantitative description of the

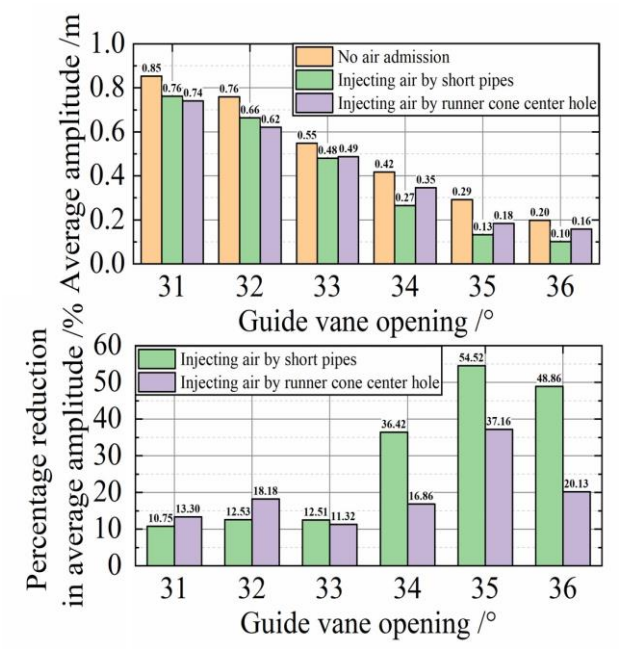

Fig. 19 Average amplitude of pressure fluctuation with different guide vane openings and the effect of air admission

overall intensity of pressure fluctuations on the draft tube wall and a comprehensive evaluation of the effect of the two types of air admission, as shown in Fig. 19.

When the guide vane opening is less than 34°, using the runner cone center hole to inject air can reduce the pressure fluctuation by up to 18.18%, while using the short pipes to inject the air can reduce by up to 12.53%. This means, under partial load conditions with a flow rate of about 0.85*Q*, using the center hole can reduce the pressure fluctuation by more. However, this measure also has the problem of not being able to reduce the amplitude at some monitoring points. In contrast, using short pipes can reduce the amplitude at almost all monitoring points. It is difficult to reduce the pressure fluctuation amplitude when the hydro-turbine is operating in partial load, especially operating near the deep partial load. Using the center hole to inject air can improve the effect, and it can also provide a new feasible idea for the study of reducing the pressure fluctuation inside the draft tube.

When the guide vane opening is greater than 33°, as in 35°, using short pipes to inject air is more effective than injecting air from the center hole. The former can reduce the amplitude of pressure fluctuation by up to 54.52%, while the latter can only reduce the amplitude by 37.16%. This indicates that when the hydro-turbine flow is closer to the rated flow, it is more suitable to use the short pipes for air admission.

4. CONCLUSION

This article presents an unsteady numerical simulation of two-phase flow in a propeller turbine using the Reynolds-averaged Navier-Stokes (RANS) equations under the homogeneous mixture assumption. The focus of the study is to analyze the impact of vortex ropes on pressure fluctuations inside the draft tube, and to evaluate additional energy loss due to air admission by entropy production theory. The effectiveness and applicability of two different designs of air admission measures have also been analyzed in this study. The study's results lead to the following conclusions:

1) The result of pressure fluctuation in the draft tube showed that, for the horizontal plane closer to the runner, the amplitude in the dominant frequency on the left side (Refer to Fig. 6) is higher. In contrast, for the horizontal plane away from the runner, the amplitude in the dominant frequency on the right side is higher. The locations where the vortex rope contacts the draft tube wall usually exhibit larger pressure gradients, leading to greater pressure fluctuations.

2) Injecting an appropriate flow rate of air into the draft tube have a positive effect by shortening the length and reducing the diameter of vortex ropes, resulting in a more uniform pressure distribution inside the draft tube. Two different methods of air admission were evaluated in this study. Using short pipes to inject air can eliminate the portion of the vortex rope below the short pipes while injecting air through the runner cone center hole can almost completely eliminate the vortex rope.

3) The entropy production theory analysis shows that additional energy loss occurs when air is injected into the draft tube. Because the air is pushed downstream by the water flow and stays in the draft tube elbow. This phenomenon impedes the flow of water, and further causes a reduction in hydraulic efficiency of about 3%-5%.

4) The two measures of air admission have different advantages. Injecting air through the runner cone center hole is better suited for the situation of small guide vane openings and low flow rates, and it can reduce the pressure fluctuation amplitude additionally. However, this method can easily disrupt the normal flow, resulting in increased pressure fluctuation amplitude in some monitoring points while decreasing in others. Injecting air through short pipes is a method with better robustness, which is better suited for part-load conditions to minimize pressure fluctuations, especially for conditions close to the rated conditions.

ACKNOWLEDGMENTS

This work is supported by the Science and Technology Program of China Huaneng Group CO., LTD. (HNKJ21-HF70).

CONFLICT OF INTEREST

The author(s) declared no potential conflicts of interest with respect to the research, authorship, and/or publication of this article.

AUTHORS CONTRIBUTION

Huanyu Wu: Methodology, Software, Investigation, Writing — original draft, preparation; **Faye Jin**: Methodology, Software; **Yongyao Luo**: Conceptualization, Methodology, Software, Investigation, Validation, Writing-Reviewing and Editing; **Yan Ge**: Investigation, Data curation; **Qingchao Wei**: Investigation, Data curation; **Chongji Zeng**: Measurement, Supervision; **Xin Liu**: Validation, Investigation; **Weili Zhang**: Methodology, Supervision; Daqing Miao: Measurement, Investigation; **Hao Bai**: Data curation, Supervision.

REFERENCES

Ardizzon, G., Cavazzini, G., & Pavesi, G. (2014). A new generation of small hydro and pumped-hydro power plants: Advances and future challenges. *Renewable and Sustainable Energy Reviews*, *31*, 746–761. https://doi.org/10.1016/j.rser.2013.12.043

Arispe, T. M., de Oliveira, W., & Ramirez, R. G. (2018). Francis turbine draft tube parameterization and analysis of performance characteristics using CFD techniques. *Renewable Energy*, *127*, 114–124. https://doi.org/10.1016/j.renene.2018.04.055

Bosioc, A. I., Susan-Resiga, R., Muntean, S., & Tanasa, C. (2012). Unsteady pressure analysis of a swirling flow with vortex rope and axial water injection in a discharge cone. *Journal of Fluids Engineering*, *134*(8). https://doi.org/10.1115/1.4007074

Cao, J., Luo, Y., Zhuang, J., Li, X., & Wang, Z. (2022). Effect of the pressure balance device on the flow characteristics of a pump-turbine. *Proceedings of the Institution of Mechanical Engineers, Part A: Journal of Power and Energy*, *236*(8), 1533–1543. https://doi.org/10.1177/09576509221097204

Favrel, A., Gomes Pereira Junior, J., Landry, C., Müller, A., Nicolet, C., & Avellan, F. (2018). New insight in Francis turbine cavitation vortex rope: Role of the runner outlet flow swirl number. *Journal of Hydraulic Research*, *56*(3), 367–379. https://doi.org/10.1080/00221686.2017.1356758

Favrel, A., Lee, N., Irie, T., & Miyagawa, K. (2021). Design of experiments applied to francis turbine draft tube to minimize pressure pulsations and energy losses in off-design conditions. *Energies*, 14(13), Article *13*. https://doi.org/10.3390/en14133894

Foroutan, H., & Yavuzkurt, S. (2014). Flow in the simplified draft tube of a francis turbine operating at partial load—part II: Control of the vortex rope. *Journal of Applied Mechanics*, *81*(6). https://doi.org/10.1115/1.4026818

Gohil, P. P., & Saini, R. P. (2016). Numerical study of cavitation in francis turbine of a small hydro power plant. *Journal of Applied Fluid Mechanics*, *9*(1), 357–365. https://doi.org/10.18869/acadpub.jafm.68.224.24080

Gong, R. Z., Qi, N. M., Wang, H. J., Chen, A. L., & Qin, D. Q. (2017). Entropy production analysis for s-characteristics of a pump turbine. *Journal of Applied Fluid Mechanics*, *10*(6), 1657–1668. https://doi.org/10.29252/jafm.73.245.27675

Goyal, R., & Gandhi, B. K. (2018). Review of hydrodynamics instabilities in Francis turbine during off-design and transient operations. *Renewable Energy*, *116*, 697–709. https://doi.org/10.1016/j.renene.2017.10.012

Ji, L., Xu, L., Peng, Y., Zhao, X., Li, Z., Tang, W., Liu, D., & Liu, X. (2022). Experimental and numerical simulation study on the flow characteristics of the draft tube in francis turbine. *Machines*, *10*(4), 230. https://doi.org/10.3390/machines10040230

Kock, F., & Herwig, H. (2004). Local entropy production in turbulent shear flows: A high-Reynolds number model with wall functions. *International Journal of Heat and Mass Transfer*, *47*(10–11), 2205–2215. https://doi.org/10.1016/j.ijheatmasstransfer.2003.11.025

Krzemianowski, Z., & Kaniecki, M. (2023). Low-head high specific speed Kaplan turbine for small hydropower – design, CFD loss analysis and basic, cavitation and runaway investigations: A case study. *Energy Conversion and Management*, *276*, 116558. https://doi.org/10.1016/j.enconman.2022.116558

Li, D., Yu, L., Yan, X., Wang, H., Shi, Q., & Wei, X. (2021). Runner cone optimization to reduce vortex rope-induced pressure fluctuations in a Francis turbine. *Science China Technological Sciences*, *64*(9), 1953–1970. https://doi.org/10.1007/s11431-021-1867-2

Li, X., Chen, Z., Fan, X., & Cheng, Z. (2018). Hydropower development situation and prospects in China. *Renewable and Sustainable Energy Reviews*, *82*, 232–239. https://doi.org/10.1016/j.rser.2017.08.090

Liu, X., Luo, Y., Presas, A., Wang, Z., & Zhou, L. (2018). Cavitation effects on the structural resonance of hydraulic turbines: failure analysis in a real francis turbine runner. *Energies*, *11*(9), Article 9. https://doi.org/10.3390/en11092320

Luo, X., Ji, B., & Tsujimoto, Y. (2016). A review of cavitation in hydraulic machinery. *Journal of Hydrodynamics*, *28*(3), 335–358. https://doi.org/10.1016/S1001-6058(16)60638-8

Luo, Y., Wang, Z., Zhang, J., Zeng, J., Lin, J., & Wang, G. (2013). Vibration and fatigue caused by pressure pulsations originating in the vaneless space for a Kaplan turbine with high head. *Engineering Computations*, *30*(3), 448–463. https://doi.org/10.1108/02644401311314376

Mao, Z., Tao, R., Chen, F., Bi, H., Cao, J., Luo, Y., Fan, H., & Wang, Z. (2021). Investigation of the starting-

up axial hydraulic force and structure characteristics of pump turbine in pump mode. *Journal of Marine Science and Engineering*, *9*(2), Article 2. https://doi.org/10.3390/jmse9020158

Menter, F. (1993). *Zonal two equation k-w turbulence models for aerodynamic flows.* 23rd Fluid Dynamics, Plasmadynamics, and Lasers Conference. American Institute of Aeronautics and Astronautics. https://arc.aiaa.org/doi/abs/10.2514/6.1993-2906

Menter, F. R. (1994). Two-equation eddy-viscosity turbulence models for engineering applications. *AIAA Journal*, *32*(8), 1598–1605. https://doi.org/10.2514/3.12149

Muhirwa, A., Cai, W. H., Su, W. T., Liu, Q., Binama, M., Li, B., & Wu, J. (2020). A review on remedial attempts to counteract the power generation compromise from draft tubes of hydropower plants. *Renewable Energy*, *150*, 743–764. https://doi.org/10.1016/j.renene.2019.12.141

Pasche, S., Avellan, F., & Gallaire, F. (2017). Part load vortex rope as a global unstable mode. *Journal of Fluids Engineering*, *139*(5). https://doi.org/10.1115/1.4035640

Qian, Z. D., Li, W., Huai, W. X., & Wu, Y. L. (2012). The effect of runner cone design on pressure oscillation characteristics in a Francis hydraulic turbine. *Proceedings of the Institution of Mechanical Engineers Part A-Journal of Power and Energy*, *226*(A1), 137–150. https://doi.org/10.1177/0957650911422865

Qian, Z., Yang, J., & Huai, W. (2007). Numerical simulation and analysis of pressure pulsation in francis hydraulic turbine with air admission. *Journal of Hydrodynamics*, *19*(4), 467–472. https://doi.org/10.1016/S1001-6058(07)60141-3

Rajan, G. K., & Cimbala, J. M. (2016). Computational and theoretical analyses of the precessing vortex rope in a simplified draft tube of a scaled model of a Francis turbine. *Journal of Fluids Engineering*, *139*(2). https://doi.org/10.1115/1.4034693

Shrestha, U., & Choi, Y. D. (2021). Suppression of flow instability in the Francis hydro turbine draft tube by J-groove shape optimization at a partial flow rate. *Journal of Mechanical Science and Technology*, *35*(6), 2523–2533. https://doi.org/10.1007/s12206-021-0523-2

Sunsheng, Y., Enema Ohiemi, I., Singh, P., Li, Y., Ali, A., & Osman, F. (2023). Numerical and experimental investigation on unsteady flow and hydraulic radial force of low-head axial flow turbine. *Journal of Applied Fluid Mechanics*, *16*(4), 830–849. https://doi.org/10.47176/jafm.16.04.1535

Yu, A., Luo, X. W., & Ji, B. (2015). Numerical simulation and analysis of the internal flow in a Francis turbine with air admission. *International Symposium of Cavitation and Multiphase Flow (Iscm 2014)*, Pts 1-6, 72, 042047. https://doi.org/10.1088/1757-899X/72/4/042047

Yu, A., Tang, Q., Zhou, D., & Liu, J. (2021a). Numerical investigation of the energy evaluation in a Francis turbine based on an advanced entropy production model. *International Communications in Heat and Mass Transfer*, *129*, 105755. https://doi.org/10.1016/j.icheatmasstransfer.2021.105755

Yu, A., Wang, Y. S., & Zhou, D. Q. (2021b). Vortex evolution and energy production in the blade Channel of a Francis Turbine Operating at Deep Part load conditions. *Journal of Applied Fluid Mechanics*, *14*(6), 1669–1678. https://doi.org/10.47176/jafm.14.06.32435

Yu, A., Zou, Z., Zhou, D., Zheng, Y., & Luo, X. (2020). Investigation of the correlation mechanism between cavitation rope behavior and pressure fluctuations in a hydraulic turbine. *Renewable Energy*, *147*, 1199–1208. https://doi.org/10.1016/j.renene.2019.09.096

Zhan, J., Chen, Z., Li, C., Hu, W., & Li, Y. (2020). Vortex identification and evolution of a jet in cross flow based on Rortex. *Engineering Applications of Computational Fluid Mechanics*, *14*(1), 1237–1250. https://doi.org/10.1080/19942060.2020.1816496

Zhang, R., Mao, F., Wu, J. Z., Chen, S. Y., Wu, Y. L., & Liu, S.-H. (2009). Characteristics and control of the draft-tube flow in part-load Francis turbine. *Journal of Fluids Engineering*, *131*(2), 021101. https://doi.org/10.1115/1.3002318

Zhou, L., Hang, J., Bai, L., Krzemianowski, Z., El-Emam, M. A., Yasser, E., & Agarwal, R. (2022). Application of entropy production theory for energy losses and other investigation in pumps and turbines: A review. *Applied Energy*, *318*, 119211. https://doi.org/10.1016/j.apenergy.2022.119211

Zhou, X., Shi, C., Miyagawa, K., & Wu, H. (2021). Effect of modified draft tube with inclined conical diffuser on flow instabilities in Francis turbine. *Renewable Energy*, *172*, 606–617. https://doi.org/10.1016/j.renene.2021.03.075

Zhou, X., Wu, H., & Shi, C. (2019). Numerical and experimental investigation of the effect of baffles on flow instabilities in a Francis turbine draft tube under partial load conditions. *Advances in Mechanical Engineering*, *11*(1), 1687814018824468. https://doi.org/10.1177/1687814018824468

Zhou, X., Wu, H., Cheng, L., Huang, Q., & Shi, C. (2023). A new draft tube shape optimisation methodology of introducing inclined conical diffuser in hydraulic turbine. *Energy*, *265*, 126374. https://doi.org/10.1016/j.energy.2022.126374

Zhu, L., Zhang, R., Yu, A., Lu, L., & Luo, X. (2021). Suppression of vortex rope oscillation and pressure vibrations in Francis turbine draft tube using various strategies. *Journal of Hydrodynamics*, *33*(3), 534–545. https://doi.org/10.1007/s42241-021-0038-4